Accelerated soil moisture drought onset link to high temperatures and asymmetric responses associated with the hit timing

Yi Liu[1,2], Zhimin Wang [1], Xinyu Zhang[1], Ye Zhu[3], Liliang Ren[1], Shanshui Yuan[1], Junliang Jin[1*]

[1]National Key Laboratory of Water Disaster Prevention, Hohai University, Nanjing, 210098, China

[2]College of Geography and Remote Sensing, Hohai University, Nanjing, 210098, China

[3]School of Hydrology and Water Resources, Nanjing University of Information Science and Technology, Nanjing, 210044, China

Correspondence to: Junliang Jin (jljin@hhu.edu.cn) and Shanshui Yuan (yuanshanshui@hhu.edu.cn)

Abstract. Frequent record high temperatures in recent years have led to a rise in both the frequency and intensity of drought events, while also altered the formation process of drought. The worldwide occurrences of flash droughts during the past decade are the evidence that drought may evolve in an unusually rapid manner. Such a change of drought challenges existing drought monitoring and early warning systems typically designed for monthly-scale purposes. This leads to a query that to what extent the formation process of drought would be accelerated under high temperatures. Based on the reanalysis product, we identified historical drought events across China during 1950－2021, and defined a new drought characteristic, the duration of drought onset (*DDO*, defined as the time period taken for moisture transition from a normal state to below-average condition) to measure how rapid the drought develops. Then a two-stage experimental framework was designed to establish the relationship between *DDO* and antecedent soil moisture, precipitation, and air temperature, and to estimate the impacts of high temperatures with different warming scenarios and varied hitting time (pre-, and post-drought onset) on *DDO*. Results showed that *DDO* would shorten by 10~50 days under 35℃ (high temperatures in meteorology) in relative to that of annual mean temperature scenarios. Overall, the impacts of high temperatures were greatest during the week of drought onset. High temperatures of pre-drought and post-drought onset exhibited asymmetrical effects on *DDO*. In high NDVI areas, pre-drought high temperatures presented a leading role for accelerating the formation of drought, while in low NDVI areas, high temperatures after drought onset were favorable for the ongoing development of drought. Findings in this study may supplement the process understanding of drought in the future warming environment.

1 Introduction

Climate change have led to high temperatures more likely. The unusual warmth in 2022 and 2023 are the recent fingerprints of the warming climate, where many countries in the Northern Hemisphere experienced the hottest summer (e.g., parts of western and northern Europe, and the Yangtze River basin in China) and the warmest September (e.g., North America) on record (van der Woude et al., 2023; Liu et al., 2023a). Such consecutive high temperatures have caused devasting impacts to human health and the welfare of the society, meanwhile, they were conducive to other climate extremes such as the wildfires and droughts (Miralles et al., 2019; Hao et al., 2022).

Much efforts have been devoted to the analysis of how drought will change in a warming climate. For example, based on the long-term historical observational data, reanalyses, and the general circulation models (GCMs) projections, a variety of studies suggested an increase in terms of the frequency, intensity, and affected area of individual drought events both at the global and regional scales (Dai, 2012; Vicente-Serrano et al., 2020). Focused on the causative linkages between high temperatures and droughts, numerous studies analyzed the characteristics of concurrent droughts and heat waves, including the frequency, trends,

magnitude, hotspot locations, and associated socioeconomic and environmental impacts of such compound events (Hao et al., 2018; Alizadeh et al., 2020; Zscheischler et al., 2020; Mukherjee and Mishra, 2021; Zhou et al., 2023), and the cascading interactions between dry and hot extremes (Mukherjee et al., 2023). The patterns of compound climate extremes can be strongly

40   different due to the varied land-atmosphere coupling strength in different climate regions, underlying surfaces, and the temporal scales considered (Teuling, 2018; Zhou et al., 2019; Schumacher et al., 2022). Moreover, from a perspective of drought monitoring, the change in the formation process of drought in a warming climate is also challenging. The widespread flash droughts around the world during the past decade are the evidence that drought may develop in a more quicker pace and strong intensity (Trenberth, 2014; Mo and Lettenmaier, 2015; Ford and Labosier, 2017; Christian et al., 2019; Qing et al., 2022; Yuan et

45   al., 2023). Such a change in drought challenges the existing drought monitoring systems typically designed for slowly-evolved drought (Otkin et al., 2022; Liu et al., 2023b). Taking the 2022 Yangtze River summer drought as an example, it only took ten days for moisture status to transfer from a normal state to severe drought (Liu et al., 2023a). Previous studies also showed the increased probability of flash droughts aggravated by the internal climate variability and anthropogenic forcings (Yuan et al., 2019; Nguyen et al., 2020; Parker et al., 2021; Qing et al., 2022). However, efforts for unraveling the formation process of

50   drought under high temperatures, particularly for the changes during the onset stage of drought, are generally rare.

For the sake of improving drought early warning capabilities and facilitating drought management and adaption strategies, it is crucial to figure out to what extent the drying process would be changed under high temperatures. The influences of record high temperatures can be strongly different given the timing of their occurrence, e.g., the boosted temperature may be favorable for drought during pre-drought periods when the moisture is in a surplus state, while the roles may be changed when transferring into

55   a water stress condition. Moreover, vegetation may modulate these interactions given the coupling nature of water, energy, and vegetation. With these in mind, in this study, we apply a modeling framework to establish the relationship between the main driving factors and the onset of drought. On this basis, comprehensive quantification on the change rate of drought onset under varied temperature scenarios were conducted. These include record high temperatures with varied timing of occurrence (pre-, and post-drought onset within two months), and sensitive tests of DDO to temperature. Finally, the modulating effects of vegetation

60   on the patterns of drought onset under varied high temperature conditions were investigated.

2 Materials and Methods

2.1 Data

The soil moisture data is from an enhanced global dataset for the land component of the fifth-generation of European reanalysis (ERA5-Land) produced by the European Center for Medium-Range Weather Forecasts (ECMWF) (Muñoz-Sabater et al., 2021).

65   This dataset has been shown improved accuracy both for the surface layer and root zone compared with other reanalysis products (Beck et al., 2021). The ERA5-Land provides hourly soil moisture estimates of four layers, i.e., 0-7 cm, 7-28 cm, 28-100 cm, and 100-289 cm, at a spatial resolution of 9 km. Meanwhile, other integrated products of varied spatial and temporal resolutions are also available. In this study, daily estimates of top three layers (depth of 1 m) during 1950 to 2021, at a spatial resolution of 0.25° were employed to represent the root zone soil moisture. In addition, the actual evapotranspiration (AET) and vapor pressure

70   deficit (VPD) derived from the ERA global reanalysis product were also collected to detect the land-atmosphere coupling strength during a drought period.

The meteorological data including daily mean precipitation (P), and the maximum, air temperature (T_{max}) of 2479 national meteorological stations, were collected from the China Meteorological Administration (http://data.cma.cn/). The data span from 1961 to 2021, and they were interpolated into a spatial resolution of 0.25° using the Kriging method by taking account of the

75   influence of elevation. These data were employed to analyze the mean precipitation and maximum temperature conditions during drought process.

The third-generation Normalized Difference Vegetation Index (NDVI3g) dataset is derived from the Advanced Very High Resolution Radiometer (AVHRR) sensor operated by the National Oceanic and Atmospheric Administration (NOAA) and is made available by the Global Inventory Modeling and Mapping Studies (GIMMS) group (https://ecocast.arc.nasa.gov/-

80   data/pub/gimms). This dataset is available from 1982 to 2022, at a time interval of 16 days and a spatial resolution of 0.083°. The NDVI data were employed to distinguish densely vegetation covered, low vegetation covered regions, and bare soils.

2.2 Methods

2.2.1 Drought Index Based on Soil Moisture Percentile

In this study, the soil moisture percentile (*SMP*) was employed to identify drought events. Given the notable geographic

85   differences and seasonality of soil moisture over China, the volumetric soil moisture content was converted to percentile value. For each grid cell, the daily soil moisture series from 1950 to 2021 were assigned to 12 subsets based on the calendar months (SM_i, i=1, 2, …, 12). For each subset, thirteen candidate theoretical probability distribution functions (available in MATLAB 2019a, including Beta, Gamma, Loglogistic, Generalized extreme value, Loglog, Weibull, Exponential, Generalized pareto, Nakagami, Birnbaum-Saunders, Normal, Ray, and Rici distributions) were employed to fit soil moisture series. The optimal

90   theoretical probability distribution was chosen when the lowest value of root-mean-square error is achieved and also passes the Kolmogorov-Smirnov test at a 95% significance level. Selection of the optimal distribution among the 13 candidate distributions is referred to Liu et al. (2023b). Drought classification is based on the United States Drought Monitoring drought classification criterion (Svoboda et al., 2002; Ford et al., 2017), where drought is classified into five categories: abnormally dry, moderate drought, severe drought, extreme drought, and exceptional drought, corresponding to the threshold of 40th, 20th, 10th, 5th, and

95   2th soil moisture percentile, respectively.

2.2.2 Identification of drought events and duration of drought onset

In this study, a drought event is recognized when all the following conditions are met: (i) the *SMP* during a drought episode is less than the 40th percentile, and the first day that *SMP* falls below the 40th percentile represents the initiation time (denoted as t_0) of the drought event, whereas the termination time (denoted as t_e) of the event is recognized when the *SMP* returns to or exceeds

100   the 40th percentile; (ii) to ensure the identified event really to be a drought, the drying process must contain the interval that *SMP* falls below the 20th percentile; (iii) short-term drought events with duration (from the initiation time to the termination time) less than one month were excluded given their limited effects on agricultural production and ecological system.

Based on the aforementioned criteria, a complete process of drought typically comprises the following stages: prior to drought onset, the onset time when *SMP* reaching a threshold for the first time, the development process (or refers to the onset stage), and

105   the recovery period. For each stage, the *SMP* may present different variation patterns in response to meteorological conditions. As shown in Fig. 1, for the onset phage, the *SMP* overall exhibits continuous reduction until reaches to the lowest value (e.g., from 25th May to 4th June). Tiny variation of the rate of water depletion may also be found in response to the current water supply and energy condition. For instance, a rapid intensification process of soil moisture can be expected under persistent high temperatures and precipitation deficits, while *SMP* may also show transient rise as a result of tiny precipitation. Previous

110   researches mostly examined drought duration, intensity, or severity, while overlooked the evolution of drought during the onset stage. Such information is more valuable for drought monitoring, early warning, and adaption strategies. In this study, we focus on the behavior of *SMP* during the onset stage to explore to what extent the drying process would be accelerated under varied

meteorological forcings. Given the category of drought severity, the duration of drought onset (DDO) is defined as the time interval between the initiation time of a drought (referred to as t_0) and the time when the moisture condition falls into moderate,

115   severe, or extreme drought (referred to as t_d), denoted as DDO_m, DDO_s, and DDO_e for short, respectively.
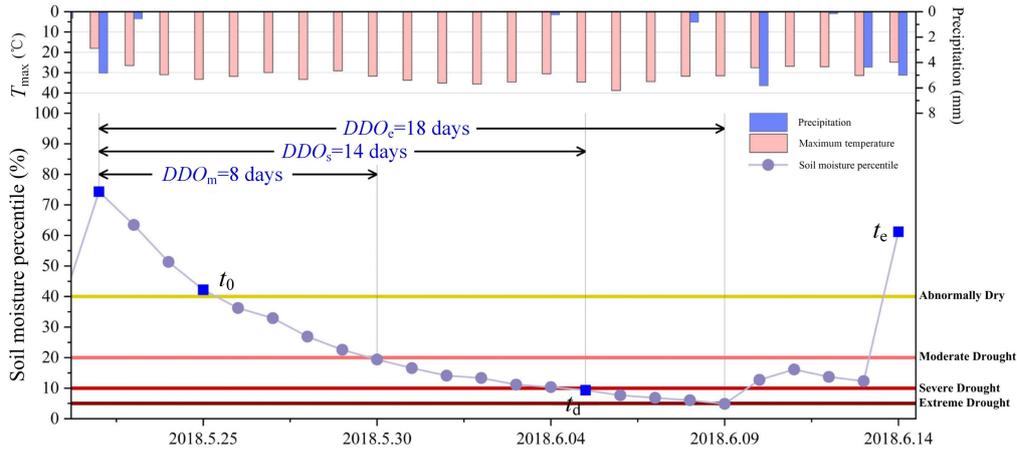
Figure 1. A schematic graph of the development process of drought. Data are from the grid cell (Beijing, 39.8°N 116.4°E). DDO_m, DDO_s, and DDO_e represent the time consumed for soil moisture percentile to reach categories of moderate, severe, and extreme drought, respectively.

2.2.3 Random Forest

120   Random forest (RF) is a machine learning technology based on a bootstrap aggregation of classification and regression trees (Cutler et al., 2012; Belgiu et al., 2016). It can be applied for classification, regression, and other tasks, with preferable ability of handling with big and high-dimensional datasets. The model generates a bootstrap sample from the original data, and trains a decision tree. All the decision trees make up a forest, and each tree in the forest has a predicted value. The final outputs of the RF method are produced by the aggregation of prediction values of all the individual trees. Compared with other machine learning

125   techniques, RF is fast, robust to noise in the predictor variables, and capable of capturing the complex nonlinear interactions between predictors and dependent variables, especially for soil moisture (Liu et al., 2022). In this study, the RF model is employed to construct the relationship between the characteristics of drought events and meteorological conditions (i.e., the explanatory variable) during the onset stage as follows:

$$Y_k = F\left(X_1, X_2, \cdots, X_n\right) \tag{1}$$

130   where Y_k can be the duration for moisture transition from abnormally dry to moderate, severe, or extreme drought, or the intensification rate of soil moisture corresponding to DDO_m, DDO_s, or DDO_e. X_1, ..., X_n are explanatory variables relevant to Y_k. In this study, the preceding soil moisture percentile at the time t_0 (refers to SMP (t_{0-1})), average precipitation (P, in unit of mm), and the maximum air temperature (T_{max}, in unit of °C) were employed as model inputs. The time period for P and T_{max} are flexible, and their average/accumulated values over a certain time period can be used as model inputs to explore the individual role or

135   accumulated effects of such variables on the formation of a soil moisture drought.

2.2.4 Experimental Design

Air temperatures of different value ranges, the occurrence time (e.g., prior to or after drought onset time), as well as their persistence may have different effects on the formation of a soil moisture drought. We designed two numerical simulation experiments to investigate the change of drought onset under varied temperature scenarios (Fig. 2). The first sets were to
140   establish the functional relationship between DDO (i.e., the predictand Y) and predictor matrix X (consist of preceding soil moisture, average precipitation, and T_{max} of varied values) during the onset stage of a drought. For the second experimental sets, we focused on the impact of high temperatures with varied timing of occurrences, i.e., pre-, at-, and post-drought onset time.

① Experimental scenario I

We first evaluated the performance of RF model for simulating DDO. The data were separated into two parts, i.e., two thirds of
145   the data for model training, and the remaining one third for model performance evaluation by using the correlation coefficient and root-mean-square error (RMSE). In this study, the tree size and the number of features were set as one thousand and three, respectively, according to the sensitivity tests of model parameters in Zhang et al. (2022). On this basis, we established a functional relationship between DDO (including DDO_m, DDO_s, and DDO_e) and preceding soil moisture, precipitation, and T_{max} as follows:

150
$$DDO = f\left(SMP(t_{0-1}), P, T_{max}\right) \qquad (2)$$

where $SMP(t_{0-1})$ represents soil moisture percentile at 1-week prior to drought onset. P refers to the average precipitation during $t_0 \sim t_d$. Although precipitation during a drought event could be negligible, there are still exceptional cases, for instance in humid regions, a drizzle may occur during a drought. T_{max} is the mean value of daily maximum air temperature during $t_0 \sim t_d$.

For experimental modeling, 400 samples of T_{max} were generated within the range of 0~40℃ at a 0.1℃ interval, to represent
155   different temperature scenarios. Considering the antecedent moisture condition corresponding to a soil moisture drought can also be different, 1000 sets of $SMP(t_{0-1})$ were randomly sampled within the range of 40th~60th percentile (representing the mildly wet condition) and 70th~90th percentile (representing the severely wet condition), respectively. Based on the probabilistic distribution of average precipitation corresponding to historical drought events, 1000 precipitation samples during the onset stage were generated by using the probability sampling method. The combination of T_{max}, $SMP(t_{0-1})$, and P samples constitute a
160   400×1000×1000 data matrix, then they were input into the RF model to explore the impacts of temperatures with different value ranges on DDO.

② Experimental scenario II

The second experimental sets aimed to explore the specific roles of high temperatures occurring in fourteen (i.e., prior to drought onset from t_{-7} to t_0, and after drought onset from t_1 to t_7) adjacent weeks of drought onset on DDO. Sampling of $SMP(t_{0-1})$ and P
165   were same as did in the experimental scenario I, while for T_{max}, its emergence time can be any interval from t_{-7} to t_7. For example, the first group aimed to explore the role of high temperatures from t_{-1} to t_0. Accordingly, 100 samples within the range of 30~40 ℃ (the sample mean was 35 ℃, which is a threshold of high temperature employed by the China Meteorological Administration) at a 0.1 ℃ interval were generated by the random sampling method for T_{max} from t_{-1} to t_0, while the remaining weeks (i.e., from t_{-7} to t_{-1} and from t_1 to t_7) of T_{max} were set as non-high temperature conditions. On this basis, we define the
170   change ratio of DDO to quantify the effect of high temperatures as follows:

$$Ratio = \frac{DDO_i - DDO_{mean}}{DDO_{mean}} \times 100\% \qquad (3)$$

where DDO_i is the simulated results of the i-th group, in other words, $T_{max}(t_0{\sim}t_i)$ is set to the scenario of high temperature. DDO_{mean} refers to the condition that air temperatures are of normal value from the period of t_{-7} to t_7 without high temperatures involved.
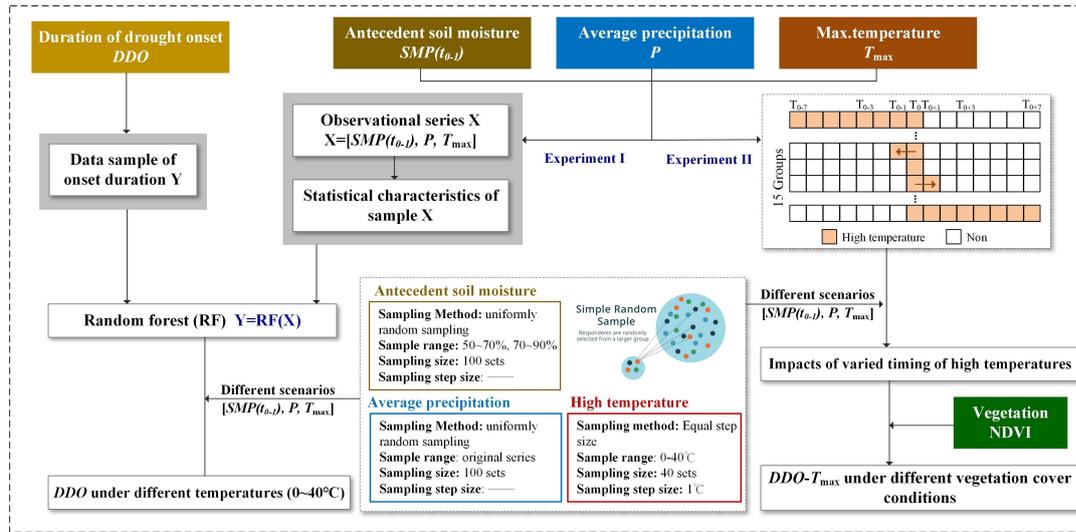
Figure 2. The flow chart of the experimental design for estimating the duration of drought onset under different temperature scenarios. DDO is the duration of drought onset, P is the average precipitation during the osnet stage of drought, $SMP(t_{0-1})$ represents the antecedent soil moisture, T_{max} represents the maximum air temperature, and RF is the random forest model.

2.3 Performance evaluation

Fig. 3 shows the correlation between drought duration (i.e., DDO_m, DDO_s, and DDO_e) during the onset stage against P, $SMP(t_{0-1})$, and T_{max}. For all three variables, higher absolute values of correlation coefficient (CC) indicate larger influences of corresponding variables on drought onset. As expected, precipitation was negatively correlated with the DDO_m, DDO_s, and DDO_e, with larger impacts in the north than in the south. Especially in the northwestern arid region, the absolute values of CC were as high as 0.6 (Fig. 3a). The antecedent soil moisture condition (i.e., $SMP(t_0)$) on the contrary, played a positive role in influencing DDO_m, DDO_s, and DDO_e, suggesting that the time period for moisture development from non-drought to drought could be long if antecedent soil moisture is sufficient. Spatially, the $SMP(t_{0-1})$ mainly influenced the northeastern China, northern China, northern Qinghai-Tibet Plateau, and the middle and lower reaches of the Yangtze River (Fig. 3b). While for other regions, the impacts of $SMP(t_{0-1})$ could be very limited given the low values of CC (no more than 0.5). Among three variables, the T_{max} showed the highest correlation with duration of drought onset. The CC values ranged between -0.4 and -0.9, with the strongest correlation in northeastern China, northern China, Qinghai-Tibet Plateau, and parts of southern China (Fig. 3c). The negative correlation suggests that the duration of drought onset is likely to be shorten under high temperatures.
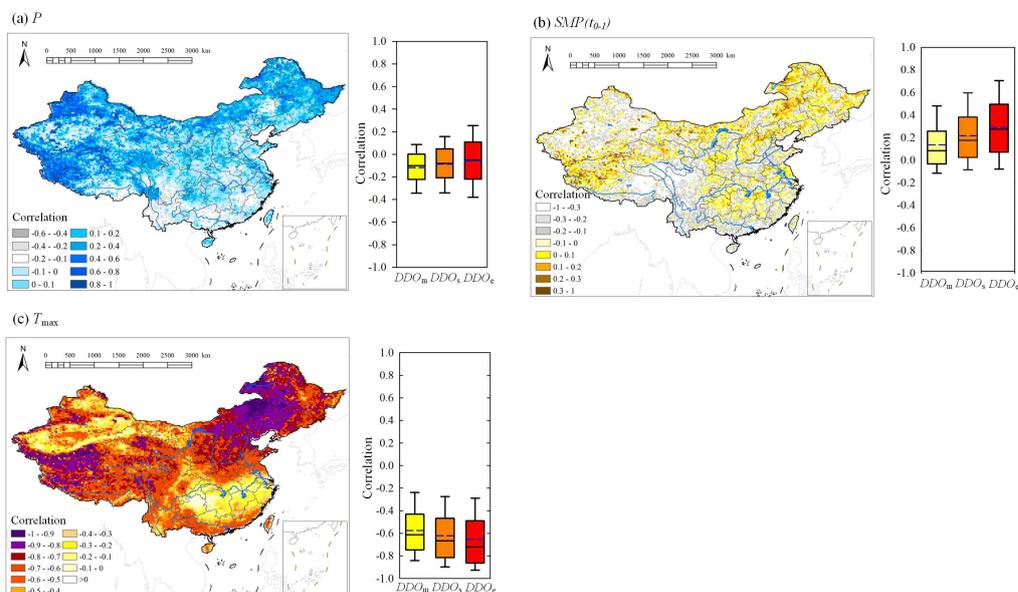
Figure 3. The spatial distribution of the CC between the DDO_s against (a) P, (b) $SMP(t_{0-1})$, and (c) T_{max}, and the boxplots shows the CC between the DDO_m, DDO_s, and DDO_e against P, $SMP(t_{0-1})$, and T_{max}, respectively.

195

We further evaluated the performance of the framework for modeling the duration of drought onset. P, $SMP(t_{0-1})$, and T_{max} were employed as inputting variables, and we simulated the DDO_m, DDO_s, and DDO_e respectively by using the RF model (the derived results were referred to as simulated duration). The performance of the RF model was evaluated by comparing simulated results with the duration derived from the ERA5-Land data (thereafter referred to as the calculated duration). Fig. 4a shows there was a good agreement between calculated duration and the RF based simulations, where the CC values were above 0.8, and the average

200   RMSE values for DDO_m, DDO_s, and DDO_e were 1 day, 3 days, and 6 days, respectively. Fig. 4b shows the spatial distribution of the mean errors of DDO_s. The lowest simulation errors (1-3 days) were found in the southern region, followed by the northern region and northeastern regions (3-5 days), and the estimation errors were of 10 days in the northwestern region.
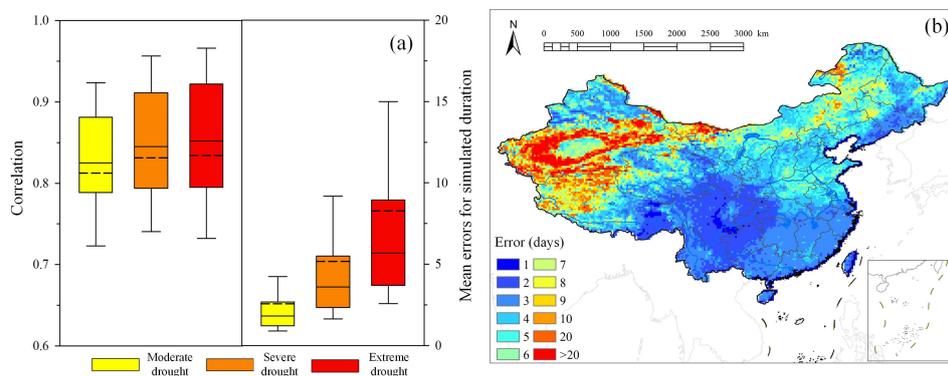
205   **Figure 4**. (a) The boxplots of CC and RMSE between calculated (from original ERA5-Land data) and simulated (by RF) DDO_m, DDO_s, and DDO_e, and (b) the spatial distribution of mean errors for simulated duration of drought onset.

3 Results

3.1 Spatiotemporal characteristics of historical drought events

Fig. 5 shows the spatial distribution of the number of drought events, mean duration, DDO_m, and DDO_s during 1950-2021 by using the ERA5-Land reanalysis data. Drought occurred more frequently (more than 500 drought events occurred) in the southern parts of the Yangtze River Basin, with peak values in the upper reaches (Chongqing and Sichuan province) where approximately 1000 drought events occurred during the past 72 years (Fig. 5a). For drought duration, drought persisted longer in the north than the south, especially for the northeastern and northwestern regions, the drought duration were 60 days or more. In contrast, the mean duration were less than 40 days in the central and southern China, especially for the Yangtze River basin, drought duration were less than 20 days (Fig. 5b). In addition, we also analyzed the duration of drought onset, i.e., the time period of moisture transition from normal to moderately dry (DDO_m) or severely dry (DDO_s). As shown in Figs. 5c and 5d, the spatial patterns of DDO_m and DDO_s were similar as in Fig. 5b, and DDO_s were approximately 5-20 days longer than DDO_m. For example, in the northeastern and northern China it on average took 15 days for the transition from a drought-free state to moderate drought (i.e., DDO_m), and the time interval doubled (more than 30 days) for DDO_s. To explore how the duration of drought onset varies over time, taking the case of DDO_s as an example, Fig. 6 presents the time series of DDO_s for all grid cells over China during 1950-2021. The boxplots show that there exists spatial heterogeneity of DDO_s over China, ranging between 5 days and 35 days, and such gaps were overall narrowed after 2002. Moreover, an evident downward pattern was found for the annual average values of DDO_s over China (blue dots in Fig. 6). This suggests that the process for the transition from drought-free status to drought on average was shorten.
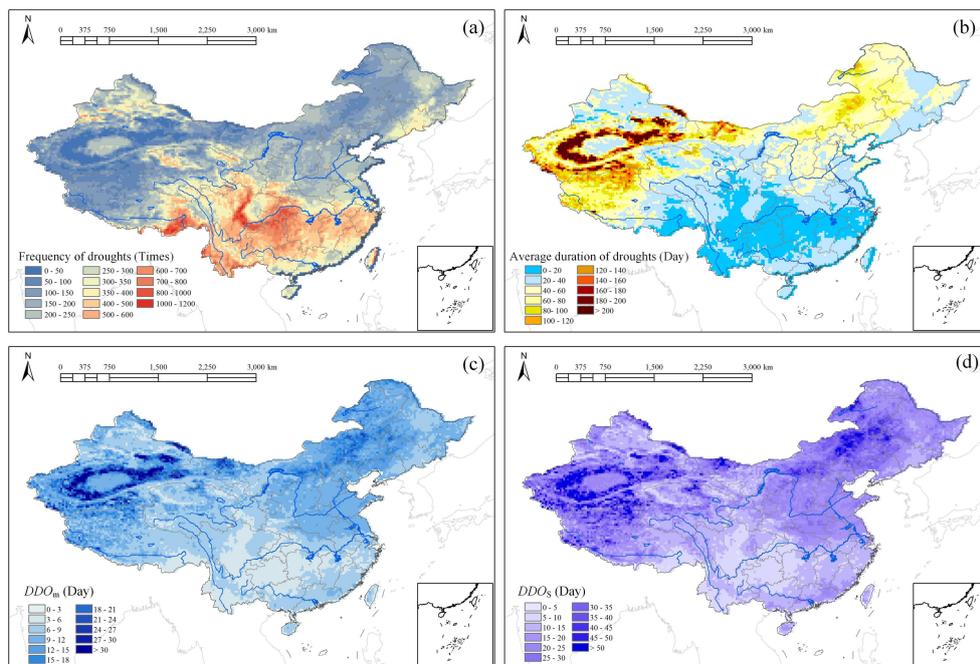
Figure 5. The spatial distribution of (a) the frequency of droughts, (b) the average duration of droughts, (c) the average time taken for reaching moderately dry (DDO_m), and (d) for reaching severely dry (DDO_s) of all drought events during 1950-2021.
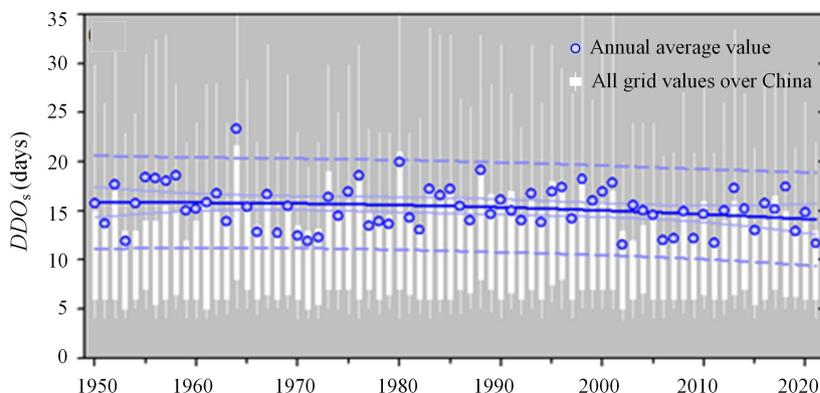
Figure 6. Boxplots of the time taken for reaching severely dry (DDO_s) of drought events for all grid cells over China during 1950-2021. The blue dots are the average values for each year.

3.2 Duration of drought onset under varied temperature scenarios

Given the evidence of accelerated formation process of drought as in Fig. 6, in this section, we make comprehensive analysis on the changes of the duration of drought onset under extreme heat conditions. The scenarios include temperature of varied values during drought onset, and the high temperatures in fourteen adjacent weeks of drought initiation. The duration of drought onset conditioned on different temperature scenarios were estimated, combined with analysis of the intervals that soil moisture is sensitive to the changes of temperature. Moreover, the timing of high temperatures, e.g., prior to or after the initiation time of drought, may have different effects on the drying of soil. We also analyzed the contribution of high temperatures in fourteen adjacent weeks of drought initiation.

3.2.1 Impacts of high temperatures and sensitive intervals

We used the RF model to explore the possible changes of the duration of drought onset by altering forcings of temperature. Fig. 7 shows the spatial distributions of the DDO under scenarios of annual mean temperature and temperature of 35℃ (this value is employed as a threshold of recognizing high temperature days by the China Meteorological Administration), respectively. The DDO_m, DDO_s, and DDO_e were 10-20 days, 30-50 days, and 60 days in the northern region under scenarios of annual mean temperature, while the values ranged between 10 and 30 days for south China. As expected, drought duration of different drought categories all significantly decreased under extreme heat conditions. For instance, DDO_m were less than 10 days in majority of China, especially for the southwestern region, DDO_m were less than 5 days. Likewise, the time period starting from abnormally dry to severe or extreme drought also decreased. The DDO_s were no more than 15 days, and DDO_e were less than 20 days except for the northwestern region. This suggests the process of soil drying could be shorten by half or one third under extreme heat conditions in relative to that of annual mean temperature scenarios.
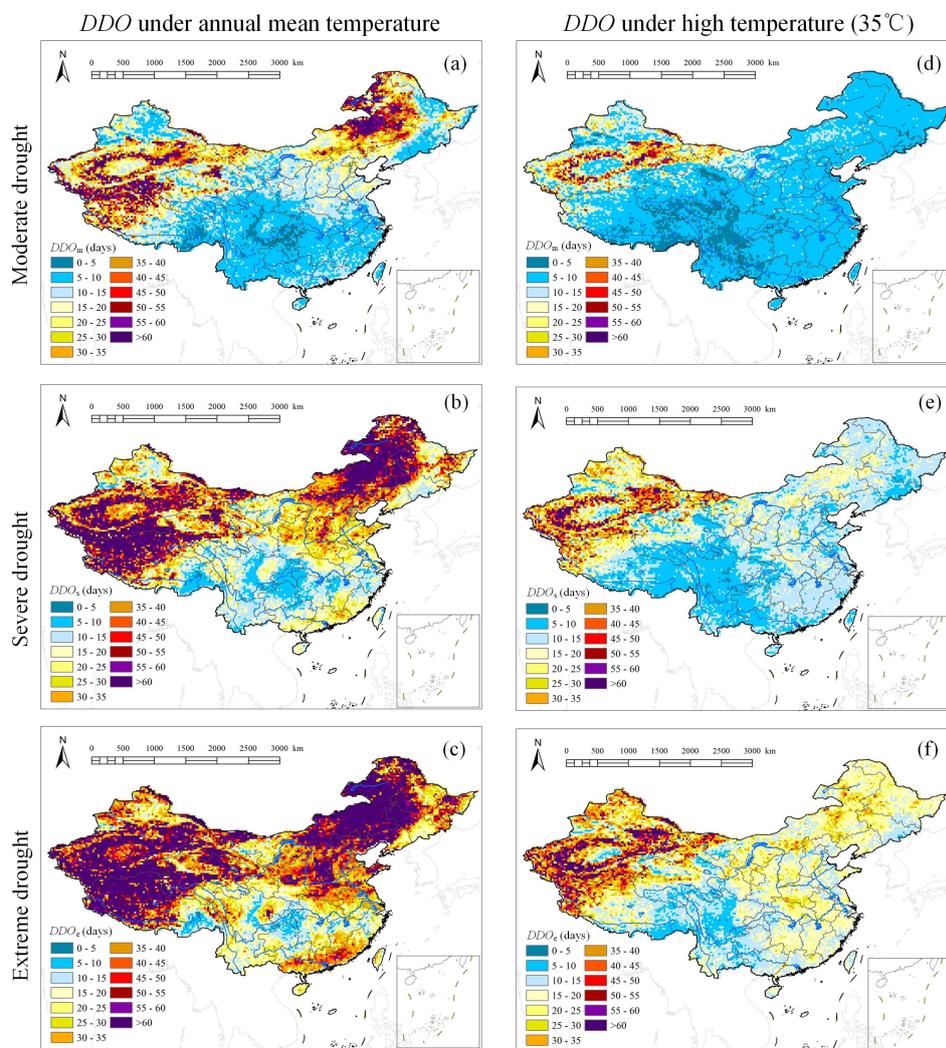
Figure 7. The spatial distribution of DDO_m, DDO_s, and DDO_e under (a~c) annual mean temperature and (d~f) temperature of 35℃.

We further explored the sensitive intervals that temperature variation may lead to marked changes for the duration of drought
255 onset. Experimental simulations were conducted for each grid cell, and the temperature scenarios were randomly sampled from the range of 0~40℃ at a 0.1℃ step. As shown in Fig. 8, the colored shades show the 25th, 75th, 95th, and 99th percentiles of drought duration under different temperature scenarios, and the white dashed lines show the average values. A general downward pattern was found for the curve of onset duration along with the temperature rises. Especially for temperature intervals of 10~15℃, the onset duration over China was shorten by 15 days on average. When temperature increased to 25℃, the DDO in
260 most regions were less than 20 days, meanwhile, the change rates of onset duration also slowed down (Fig. 8a). Regional patterns were similar as that of the nationwide, but their sensitive ranges of temperature were different. For instance, the sensitive intervals for the northeastern region were between 5℃ and 25℃, where the DDO decreased from 50~100 days to 10~30 days (Fig. 8b). In North China, the curve presented no obvious changes till temperature reached 8℃, and the onset duration approximately decreased by two thirds (from 30~50 days to 10~20 days) under temperature scenarios of 8~15℃ (Fig. 8c). Such

sharp drops of onset duration were also found in Southwest China and the southern parts of Tibet-Plateau, ranged between intervals of 15~25℃ (Fig. 8e), and 6~17℃ (Fig. 8f), respectively. The onset duration in South China on the whole was shorter than other regions, and evident decreases of onset duration were found at intervals between 20℃ and 35℃ (Fig. 8d). These suggest that high temperatures may accelerate the formation process of soil moisture drought, meanwhile, its role may also be finite and would not influence the drying process a lot when exceeding the sensitive intervals in different regions.region, and the white dashed lines show the average values of the duration of drought onset.
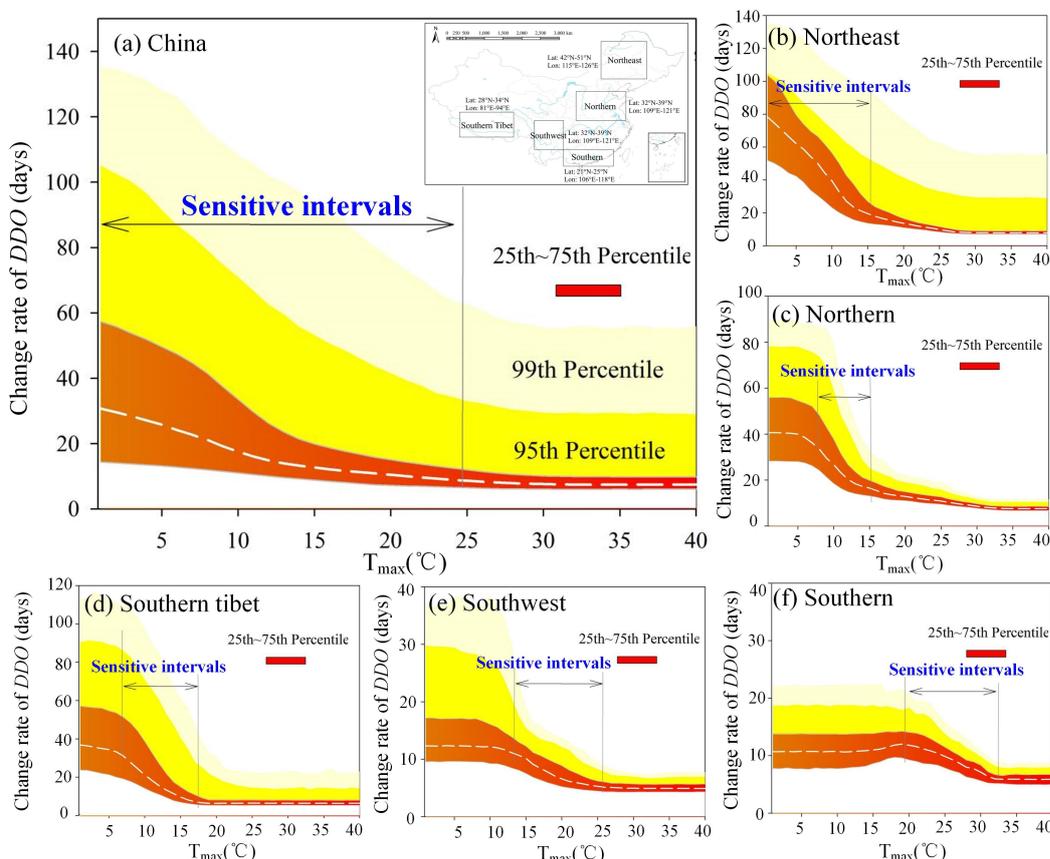
Figure 8. The change rate of drought onset under different temperature scenarios (a) over China and in (b) Northeast: 115°E-126°E, 42°N-51°N; (c) Northern: 109°E-121°E, 32°N-39°N; (d) Southern Tibet: 81°E-91°E, 28°N-34°N; (e) Southwest: 99°E-106°E, 25°N-32°N; (f) Southern: 106°E-118°E, 21°N-25°N China. The colored shades show the 25th, 75th, 95th, and 99th percentiles of the duration of drought onset under temperature scenarios for grid cells in each region, and the white dashed lines show the average values of the duration of drought onset.

3.2.2 Impacts of varied timing of high temperatures

The timing of high temperatures is also crucial for drought development. Before drought initiation, the soil is typical in a normal or wet state, which allows for a higher rate of evapotranspiration to meet the atmospheric demands. In this circumstance, predrought high temperatures are expected to play a positive role in accelerating the formation process of drought. As the drought proceeds, the role of high temperatures may also change along with a transition from water surplus to water deficit (Budyko, 1974; Roderick et al., 2009). On these grounds, we analyzed the change rate of DDO under high temperatures occurring in fourteen adjacent weeks of drought initiation. As shown in Fig. 9, the probability distribution curve refers to the change ratio of

DDO caused by high temperatures randomly sampling within the range of 30~40°C during the period of T_0~T_i for all grid cells over China. Positive change rates of *DDO* indicate that high temperatures promote the drying process of soil profile, namely the

285 *DDO* becomes less compared to those under normal temperature condition, and vice versa for negative values. Overall, high temperatures in fourteen adjacent weeks of drought initiation (namely T_0) all show a positive role for drying the soil with the mean change rates of *DDO* above 15%. Specifically, for periods before drought initiation, the *DDO* on average would be shorten by 25% with high temperatures occurring in four consecutive weeks (namely from T_{-4} to T_0) prior to drought initiation. Then the change rate of *DDO* generally decreases as the period of high temperatures shortens, and drops to 15% when high temperatures

290 exactly occur in T_0. In contrast, more prominent effects of high temperatures were found for periods after drought initiation. For example, the *DDO* on average would be shorten by 30% with high temperatures during T_0~T_1, and such effects of promoting soil drying would be further enhanced with continuously lengthened time intervals of high temperatures from T_0 to T_4 (the mean change rate was approximately 55%). For periods of one month after drought initiation, the *DDO* would no longer change as the time intervals of high temperatures lengthened.
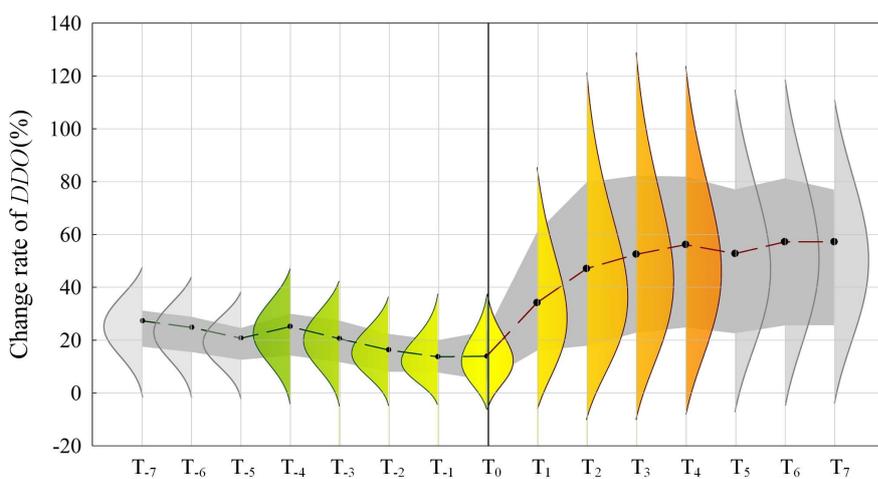
295

Figure 9. The change rate of *DDO* caused by high temperatures occurring at different time intervals (from T_0 to T_i, and $i \neq 0$ and is an integer ranging from -7 to 7), which was averaged over all grid cells in China. The probability distribution curve for *i*-th time refers to the change rate of *DDO* caused by high temperatures randomly sampling within the range of 30~40°C during the period of T_0~T_i. The dark gray stripe represents the 25th to 75th percentiles of each probability distribution, and the black solid dots show the means of the probability distribution.

300 The colored probability distributions show the effective time intervals of high temperatures on the formation process of drought.

3.3 Drought onset under varied vegetation conditions

The formation processes of drought under different high temperature scenarios are subjected to the water and energy exchanges between the atmosphere and land surface (Durre et al., 2000), and vegetation plays a fundamental role in modifying this physical process. For example, vegetation is supposed to contribute to the depletion of soil moisture by water uptake from the deep soil for

305 transpiration under sufficient water supply states, while it may also impede further soil moisture consumption by means of stomatal closure when entering into a water stress period (Yang et al., 2018). In addition, the role of vegetation becomes more complicated on account of vegetation type or density.

We use the NDVI (a comprehensive indicator of vegetation density, class, and health condition) to classify the *DDO* driven by high temperatures, and three typical regions with different vegetation greenness were extracted for comparison. As shown in Fig.

310   10, the northwest China is characterized by low NDVI values (around 0.1, generally corresponds to barren areas of rock, sand, or snow), and high temperatures after drought initiation show positive effects (Fig. 10b). With overall higher NDVI (around 0.4, corresponding to shrub, grassland, and mixed forest classes of medium vegetation density) in northeast China, the positive effects of high temperatures on DDO were extended to predrought periods (Fig. 10c). The southwest China (the NDVI is around 0.6, corresponding to the forest class with high vegetation density) exhibited more stronger positive effects during predrought periods,

315   where the DDO could be reduced by one-fold under high temperatures from T_{-7} to T_0, meanwhile, the effects of high temperatures greatly discounted after a drought initiated (Fig. 10d).
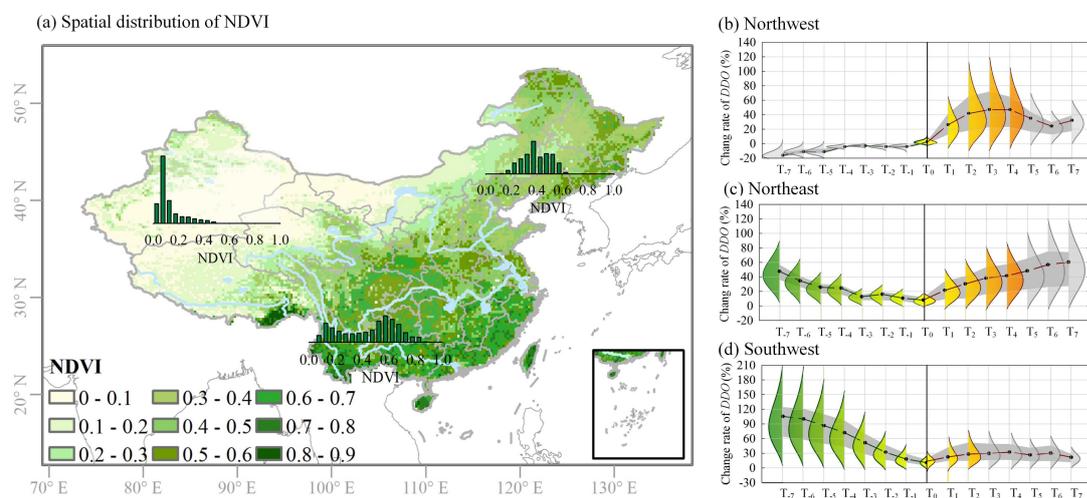
Figure 10. Spatial distribution of (a) NDVI over China and the change rate of DDO as in Fig. 9 but for (b) northwest, (c) northeast, and (d) southwest regions. The histograms show the distribution of NDVI of all grid cells in Northwest, Northeast, and Southwest China.

320

Similar patterns were also found for the change rates of DDO classified by NDVI values from 0 to 1 at an interval of 0.1 over China, where the positive effects of high temperatures during predrought periods tends to be weaker as the NDVI decreases (Fig. 11). For instance, in high NDVI areas ($0.5 \leq NDVI < 1$), predrought high temperatures exhibited an overwhelming role on DDO (Figs. 11a-d, Fig. 10d). In medium NDVI areas ($0.4 \leq NDVI < 0.5$), high temperatures exhibited parallel effects during predrought

325   and after drought periods (Fig. 11e), while for low NDVI areas ($0 < NDVI < 0.4$), positive effects of high temperatures emerged after drought initiation (Figs. 11f-i).
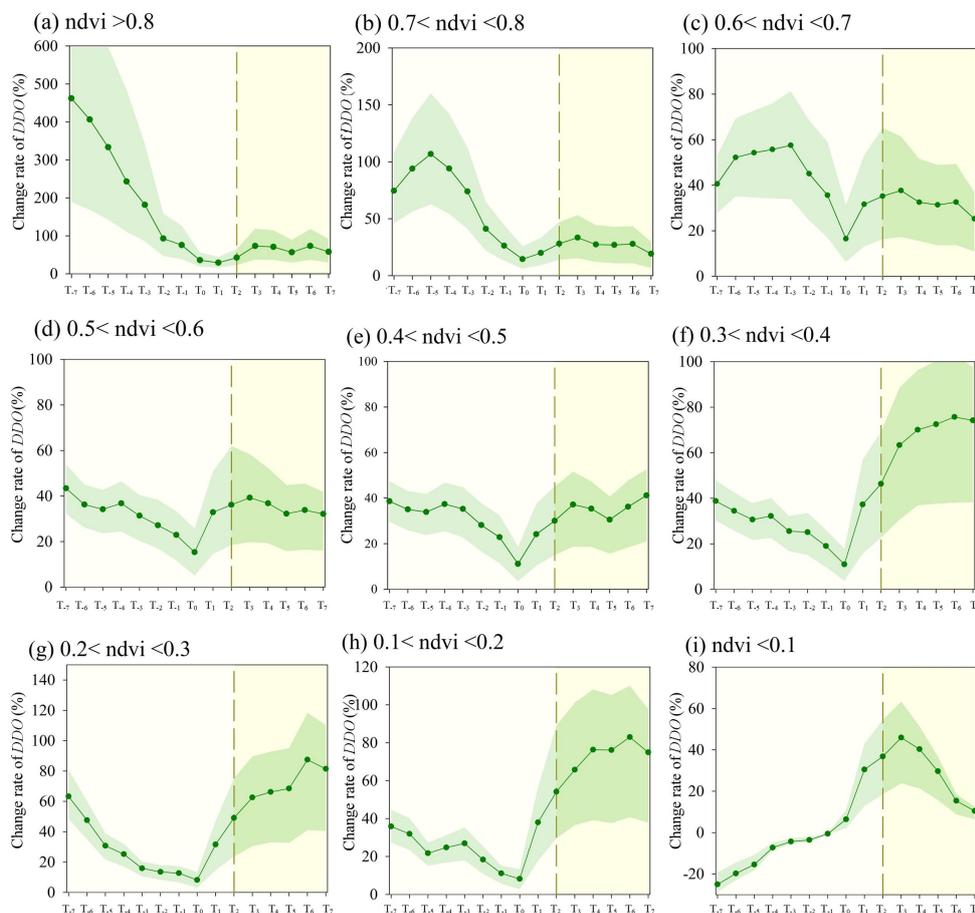
Figure 11. As in Fig. 9 but for the change rate of *DDO* under different NDVI values. The dotted vertical line in each panel shows the initiation time of a drought, the green dots are the mean change rate of *DDO* under high temperatures from T_0 to T_i, and the green shades show the range of 25th ~ 75th percentiles of the change rate of *DDO*.

To explore the reasons for the different patterns between vegetation conditions, we further compare the anomalies of *AET* (to make *AET* in different regions are comparable) in high and low NDVI areas. As shown in Fig. 12a, the high NDVI regions exhibited stronger positive *AET* anomalies than in low NDVI areas at two week leads, suggesting that vegetation of high density and fraction (roughly corresponds to high NDVI values) may respond more drastically to the elevated temperature and evaporative demand, resulted in increased evapotranspiration and the accelerating depletion of root zone soil moisture. A similar phenomenon was also found in Osman et al. (2022). It is worth noting that such positive effects of vegetation in response to high temperatures may largely weaken as the moisture status transfers into a water stress condition. This is evident by the sharply decreased *AET* anomalies after drought initiation in high NDVI areas. Moreover, the coupling strength between *VPD* and soil moisture also indicates the changing role of vegetation within a drying period (Seneviratne et al., 2010). As shown in Fig. 12b, high NDVI areas exhibited stronger coupling strength than the low NDVI areas, which implies the important roles of vegetation in regulating these processes. Meanwhile, in high NDVI areas, the coupling of *VDP* and soil moisture was stronger during

predrought (i.e., energy limited) periods than after drought (i.e., water limited) periods. In contrast, there virtually no changes within a drying period for low NDVI areas. This to some extent explains why predrought high temperatures presented more prominent effects in high NDVI areas, while the role of vegetation in low NDVI areas were very limited.
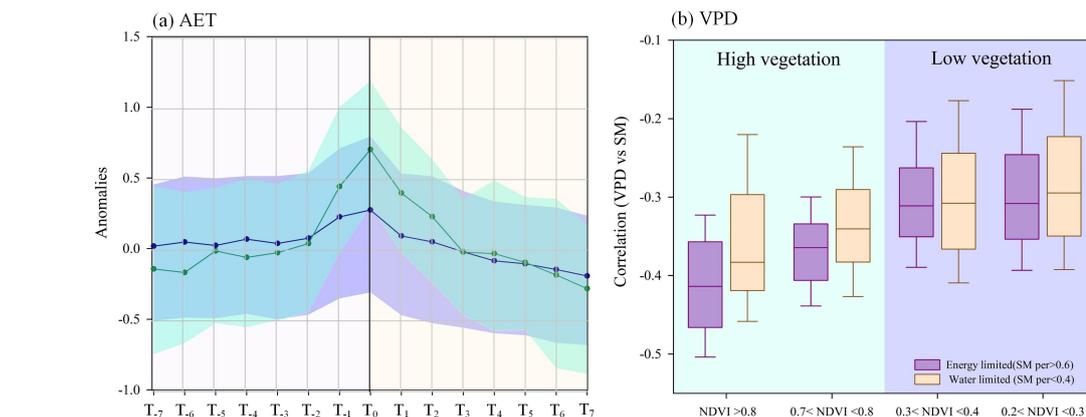
Figure 12. (a) Variation of *AET* anomalies in high ((NDVI > 0.7) and low (0.2<NDVI<0.3) NDVI areas in fourteen adjacent weeks of drought initiation (T_0). The green and purple shadows in **(a)** are the 25th percentile to 75th percentile of *AET* anomalies in high and low NDVI areas, respectively, and the two circle chains are corresponding means of *AET* anomalies. (b) Boxplots of the correlation between *VPD* and soil moisture during predrought (purple box) and after drought (orange box) periods in high and low NDVI areas.

4 Discussion and Conclusions

Frequent occurrences of record high temperatures around the world have motivated efforts to the spatiotemporal patterns, causal analysis, and associated social and ecological impacts of the dry and hot extremes (Mazdiyasni and AghaKouchak, 2015; Williams et al., 2015; Naumann et al,. 2021; Yin et al., 2023). For the case of drought, the resulting changes in a warming climate are not confined to typical drought characteristics such as drought frequency and intensity (Otkin et al., 2018; Chiang et al., 2021; Lian et al., 2021; Wang et al., 2021), while the change of drought evolution process is also challenging.

In this study, we focused on the development of drought during the onset stage, which was defined as the time period of moisture transferring from a normal state to moderate, severe, or extreme drought (referred to as the *DDO* in this study). Comparing to previous researches that characterize flash drought from a perspective of intensification rate (e.g., Otkin et al., 2022; Liu et al., 2020), the *DDO* is operational-friendly by providing more intuitive information on the specific days consumed for the onset of a flash drought, which may facilitate policy makers to incorporate such information into the early-warning and drought monitoring system without additional data processing. Certainly, *DDO* can also be transformed into the intensification rate as did in previous researches.

The results suggest *DDO* on average would be shorten by 10~50 days under 35°C (a threshold of high temperature in meteorology) in relative to that of annual mean temperature scenarios, with most evident changes in the middle and eastern parts of northeast China, and north China (Fig. 7). This implies with more frequent high temperatures in the future, such as the globally record-high temperatures in the 2022 and 2023 summer, droughts over China may have faster onset than present (Yuan et al., 2019). As a result, the northeast and north China which were recognized as low-frequent flash drought regions in previous studies (e.g., Wang et al., 2016; Liu et al., 2020), also have potential increments of flash droughts under the warming climate. In addition, it should be noted that *DDO* does not continuously change as the rising temperature, even for south China which presents highest

sensitivity to high temperatures (Fig. 8). This could relate to the limited data samples of temperatures above 35 ℃ or 40 ℃ (generally rare in historical events for most regions over China) for model training, which may reduce the simulation accuracy and lead to the boundary effect. In addition, the role of temperature could also be very limited when reaching a rather high value, while other aerodynamic fluxes may be more crucial for the ongoing development of soil moisture drought (Christian et al.,

375   2024).

Meanwhile, the role of high temperatures was shown to be strongly different given the timing of their occurrence (Fig. 9). For the whole China, high temperatures of 1-month leads were most relevant to soil drying, and could be employed as a precursor of rapid drought onset. As drought evolves, the water and thermal forces also changes, high temperatures after drought onset were also conductive to the ongoing process of soil moisture drought, and such promoting effects may persist for one month. In other

380   words, high temperatures at one month interval to drought onset are effective for accelerating soil drying over China.

During the shift of driving forces from water control to thermal control, vegetation also modulates the water and energy balances between the atmosphere and land surface (Vanloon, 2015; Warter et al., 2021), leading to different roles of high temperatures under varied vegetation conditions. In high NDVI areas such as the southwest China, pre-drought high temperatures contributed to a higher evapotranspiration rate by means of water uptake from soil (Fig. 12), and were conductive to the formation of soil

385   moisture drought. However, when the soil moisture enters into water deficiency state (after drought initiation), evapotranspiration would not continuously increase under high temperatures, rather high temperatures may arise the stomatal closure of vegetation to impede further water losses from the soil (Seneviratne et al., 2010). This is evident by the sharply decreased AET anomalies after drought initiation (Fig. 12a) and also weakened coupling of VPD and soil moisture (Fig. 12b). However, in low NDVI areas such as the northwest China, high temperatures after drought initiation played a leading role in accelerating the development of

390   soil moisture drought. This shows the asymmetrical effects between pre-drought and post-drought high temperatures on DDO. Therefore, it is necessary to take account of regional differences associated with high temperature roles when making local drought early warning, drought monitoring, and prediction related strategies.

Findings in this study supplement the understanding of the change rate of drought formation in a warming process. Given the evidence of accelerated drought onset under warming scenarios, it is recommended to incorporate the formation of drought

395   during the onset stage in future drought assessments, as did for drought intensity and duration.

Acknowledgments

This study was supported by the National Natural Science Foundation of China under Grant No. (42171021, U2243203); the National Key Research and Development Program (2023YFC3209800); the National Natural Science Foundation of Jiangsu Province Youth Fund, under Grant BK 20220145.

400   **Data Availability**

The daily meteorological data were collected from the China Meteorological Administration (http://data.cma.cn/). ERA5-Land data used in this study are available through European Centre for Medium-Range Weather Forecasts (https://cds.climate.copernicus.eu/). The third-generation Normalized Difference Vegetation Index (NDVI3g) dataset was obtained from the National Aeronautics and Space Administration (NASA) Ames Ecological Forecasting Lab

405   (https://ecocast.arc.nasa.gov/data/pub/gimms/3g.v1/). The software is Matlab (version 2019a), and the function packages can be downloaded from the website (https://www.mathworks.com).

Author contribution

Author contributions. ZW carried out the analyses, wrote the manuscript. XZ prepared the figures and data. YL and LR designed the paper and supervised the formulation of this manuscript. YZ provided critical feedback and edits. JJ and SY provided
410   important suggestions. All authors discussed the results and contributed to the final paper.

Competing interests

 The contact author has declared that none of the authors has any competing interests.

References

Alizadeh, M. R., Adamowski, J., and Nikoo, M. R.: A century of observations reveals increasing likelihood of continental-scale
415   compound dry-hot extremes, Sci. Adv., 6, eaaz4571, https://doi.org/10.1126/sciadv.aaz4571, 2020.

Beck, H.E., Pan, M., and Miralles, D.G.: Evaluation of 18 satellite- and model-based soil moisture products using in situ measurements from 826 sensors, Hydrol. Earth Syst. Sci., 25, 17-40, https://doi.org/10.5194/hess-25-17-2021, 2021.

Belgiu, M. and Drăguţ, L.: Random forest in Remote Sens.-Basel: A review of applications and future directions, ISPRS J. Photogramm. Remote Sens., 144, 24-31, https://doi.org/10.1016/j.isprsjprs.2016.01.011, 2016.

420   Budyko, M. I.: New York, NY: Academic Press, Climate and life, p. 508, 1974.

Chiang, F., Mazdiyasni, O., and AghaKouchak, A.: Evidence of anthropogenic impacts on global drought frequency, duration, and intensity, Nat. Commun., 12, 2754, https://doi.org/10.1038/s41467-021-22314-w, 2021.

Christian, J. I., Basara, J. B., and Otkin, J. A.: A methodology for flash drought identification: Application of flash drought frequency across the United States, J. Hydrol., 20, 833–846, https://doi.org/10.1175/JHM-D-18-0198.1, 2019.

425   Christian, J. I., Hobbins, M., and Hoell, A.: Flash drought: A state of the science review, WIRES Water., 11(3), e1714, https://doi.org/10.1002/wat2.1714, 2024.

Cutler, A., Cutler, D.R., and Stevens, J.R.: Random Forests. In: Zhang, C., Ma, Y. (Eds.), Ensemble Machine Learning (pp. 157-175), New York, NY: Springer, https://doi.org/10.1007/978-1-4419-9326-7_5, 2012.

Dai, A.: Increasing drought under global warming in observations and models, Nat. Clim. Change, 3, 52-58,
430   https://doi.org/10.1038/nclimate1633, 2012.

Durre, I., Wallace, J. M., and Lettenmaier, D. P.: Dependence of extreme daily maximum temperatures on antecedent soil moisture in the contiguous United States during summer, J. Climate, 13, 2641-2651, https://doi.org/10.1175/1520-0442(2000)013<2641:DOEDMT>2.0. CO;2, 2000.

Ford, T. W. and Labosier, C. F.: Meteorological conditions associated with the onset of flash drought in the eastern United States,
435   Agr. Forest Meteorol., 247, 414-423, https://doi.org/10.1016/j.agrformet.2017.08.031, 2017.

Hao, Z., Hao, F., and Singh, V. P.: Changes in the severity of compound drought and hot extremes over global land areas, Environ. Res. Lett., 13, https://doi.org/10.1088/1748-9326/aaee96, 2018.

Hao, Z., Hao, F., and Xia, Y.: Compound droughts and hot extremes: Characteristics, drivers, changes, and impacts, Earth-Sci. Rev., 235, 104241, https://doi.org/10.1016/j.earscirev.2022.104241, 2022.

440   Lian, X., Piao, S., and Chen, A.: Multifaceted characteristics of dryland aridity changes in a warming world, Nat. Rev. Earth Env., 2, 232–250, https://doi.org/10.1038/s43017-021-00144-0, 2021.

Liu, Y., Chen, R., and Yuan, S.: Satellite Soil Moisture Data Reconstruction in the Temporal and Spatial Domains: Latent Error Assessments and Performances for Tracing Rainstorms and Droughts, Remote Sens.-Basel, 14(19), 4841, https://doi.org/10.3390/rs14194841, 2022.

445   Liu, Y., Yuan, S., and Zhu, Y.: The patterns, magnitude, and drivers of unprecedented 2022 mega-drought in the Yangtze River Basin, China, Environ. Res. Lett., 18(11): 114006, https://doi.org/10.1088/1748-9326/acfe21, 2023a.

Liu, Y., Zhu, Y., and Ren, L.: Flash drought fades away under the effect of accumulated water deficits: the persistence and transition to conventional drought, Environ. Res. Lett., 18(11), 114035, https://doi.org/10.1088/1748-9326/acfccb, 2023b.

Liu, Y., Zhu, Y., and Zhang, L.: Flash droughts characterization over China: From a perspective of the rapid intensification rate,
450   Sci. Total Environ., 704, 135373, https://doi.org/10.1016/j.scitotenv.2019.135373, 2020.

Mazdiyasni, O. and AghaKouchak, A.: Substantial increase in concurrent droughts and heatwaves in the United States, P. Natl. A. Sci. India B. , 112 (37), 11484–11489, https://doi.org/10.1073/pnas.1422945112, 2015.

Miralles, D. G., Gentine, P., and Seneviratne, S. I.: Land–atmospheric feedbacks during droughts and heatwaves: state of the science and current challenges, Ann. Ny. Acad. Sci., 1436(1), 19-35, https://doi.org/10.1111/nyas.13912, 2019.

455   Mo, K. C. and Lettenmaier, D. P.: Heat wave flash droughts in decline, Geophys. Res. Lett., 42(8), 2823-2829, https://doi.org/10.1002/2015GL064018, 2015.

Mukherjee, S., Mishra, A. K., and Zscheischler, J.: Interaction between dry and hot extremes at a global scale using a cascade modeling framework, Nat. Commun., 14(1), 277, https://doi.org/10.1038/s41467-022-35748-7, 2023.

Mukherjee, S. and Mishra, A. K.: Increase in compound drought and heatwaves in a warming world, Geophys. Res. Lett., 48(1),
460   e2020GL090617, https://doi.org/10.1029/2020GL090617, 2021.

Muñoz-Sabater, J., Dutra, E., and Agustí-Panareda, A.: ERA5-Land: A state-of-the-art global reanalysis dataset for land applications, Earth Syst. Sci. Data, 13(9), 4349-4383, https://doi.org/10.5194/essd-13-4349-2021, 2021.

Naumann, G., Cammalleri, C., and Mentaschi, L.: Increased economic drought impacts in Europe with anthropogenic warming, Nat. Clim. Change, 11, 485–491, https://doi.org/10.1038/s41558-021-01044-3, 2021.

465   Nguyen, H., Otkin, J. A., and Wheeler, M. C.: Climatology and variability of the evaporative stress index and its suitability as a tool to monitor Australian drought, J. Hydrometeology, 21, 2309-2324, https://doi.org/10.1175/JHM-D-20-0042.1, 2020.

Osman, M., Zaitchik, B. F., and Winstead, N. S.: Cascading Drought-Heat Dynamics During the 2021 Southwest United States Heatwave, Geophys. Res. Lett., 49(12), e2022GL099265, https://doi.org/10.1029/2022GL099265, 2022.

Otkin, J. A., Svoboda, M., and Hunt, E. D.: Flash droughts: A review and assessment of the challenges imposed by rapid-onset
470   droughts in the United States, B. Am. Meteorol. Soc., 99, 911–919, https://doi.org/10.1175/BAMS-D-17-0149.1, 2018.

Otkin, J. A., Woloszyn, M., and Wang, H.: Getting ahead of flash drought: from early warning to early action, B. Am. Meteorol. Soc., 103(10), E2188-E2202, https://doi.org/10.1175/BAMS-D-21-0288.1, 2022.

Parker, T., Gallant, A., and Hobbins, M.: Flash drought in Australia and its relationship to evaporative demand, Environ. Res. Lett., 16(6), 064033, https://doi.org/10.1088/1748-9326/abfe2c, 2021.

475   Qing, Y., Wang, S., and Ancell, B. C.: Accelerating flash droughts induced by the joint influence of soil moisture depletion and atmospheric aridity, Nat. Commun., 13,1139, https://doi.org/10.1038/s41467-022-28752-4, 2022.

Roderick, M. L., Hobbins, M. T., and Farquhar, G. D.: Pan evaporation trends and the terrestrial water balance II, Energy balance and interpretation, Geography Compass, 3(2), 761–780, https://doi.org/10.1111/j.1749-8198.2008.00214.x, 2009.

Schumacher, D. L., Keune, J., and Dirmeyer, P.: Drought self-propagation in drylands due to land–atmosphere feedbacks, Nature
480   geoscience, 15, 262-268, https://doi.org/10.1038/s41561-022-00912-7, 2022.

Seneviratne, S. I., Corti, T., and Davin, E. L.: Investigating soil moisture–climate interactions in a changing climate: A review, Earth-Sci. Rev., 99, 125–61, https://doi.org/10.1016/j.earscirev.2010.02.004, 2010.

Svoboda, M., LeComte, D., and Hayes, M.: The drought monitor, B. Am. Meteorol. Soc., 83(8), 1181-1190, https://doi.org/10.1175/1520-0477-83.8.1181, 2002.

485 Teuling, A. J.: A hot future for European droughts, Nat. Clim. Change, 8(5), 364-365, https://doi.org/10.1038/s41558-018-0154-5, 2018.

Trenberth, K. E., Dai, A., and Van Der Schrier, G.: Global warming and changes in drought, Nat. Clim. Change, 2014, 4(1): 17-22, https://doi.org/10.1038/nclimate2067, 2014.

Van Der Woude, A. M., Peters, W., and Joetzjer, E.: Temperature extremes of 2022 reduced carbon uptake by forests in Europe, 490 Nat. Commun., 14(1), 6218, https://doi.org/10.1038/s41467-023-41851-0, 2023.

Van Loon, A. F.: Hydrological drought explained, WIRES Water., 2(4), 359-392, https://doi.org/10.1002/wat2.1085, 2015.

Vicente-Serrano, S. M., Quiring, S. M., and Peña-Gallardo, M.: A review of environmental droughts: Increased risk under global warming? Earth-Sci. Rev., 201, 102953, https://doi.org/10.1016/j.earscirev.2019.102953, 2020.

Wang, L., Yuan, X., and Xie, Z.: Increasing flash droughts over China during the recent global warming hiatus, Sci. Rep.-UK, 6, 495 30571, https://doi.org/10.1038/srep30571, 2016.

Wang, T., Tu, X., and Singh, V.P.: Global data assessment and analysis of drought characteristics based on CMIP6, J. Hydrol., 596, 126091, https://doi.org/10.1016/j.jhydrol.2021.126091, 2021.

Warter, M. M., Singer, M. B., and Cuthbert, M. O.: Drought onset and propagation into soil moisture and grassland vegetation responses during the 2012-2019 major drought in Southern California, Hydrol. Earth Syst. Sci., 25, 3713-500 3729,https://doi.org/10.5194/hess-25-3713-2021, 2021.

Webster, R. and Oliver, M. A.: Chichester, UK: John Wiley & Sons, Ltd, Geostatistics for Environmental Scientists, https://doi.org/10.1002/9780470517277, 2001.

Williams, A. P., Seager, R., and Abatzoglou, J. T.: Contribution of anthropogenic warming to California drought during 2012-2014, Geophys. Res. Lett., 42(16), 6819-6828, https://doi.org/10.1002/2015GL064924, 2015.

505 Yang, L., Wen, K. S., and Ruan, X.: Response of plant secondary metabolites to environmental factors, Molecules, 23(4), 762, https://doi.org/10.3390/molecules23040762, 2018.

Yin, J., Gentine, P., and Slater, L.: Future socio-ecosystem productivity threatened by compound drought-heatwave events, Nat. Sustain., 6, 259-272, https://doi.org/10.1038/s41893-022-01024-1, 2023.

Yuan, X., Wang, L., and Wu, P.: Anthropogenic shift towards higher risk of flash drought over China, Nat. Commun., 10, 4661, 510 https://doi.org/10.1038/s41467-019-12692-7, 2019.

Yuan, X., Wang, Y., and Ji, P.: A global transition to flash droughts under climate change, Science, 380(6641), 187-191, doi:10.1126/science.abn6301, 2023.

Zhang, L., Liu, Y., and Ren, L.: Analysis of flash droughts in China using machine learning, Hydrol. Earth Syst. Sci., 26, 3241–3261, https://doi.org/10.5194/hess-26-3241-2022, 2022.

515 Zhou, S., Williams, A. P., and Berg, A. M.: Land–atmosphere feedbacks exacerbate concurrent soil drought and atmospheric aridity, P. Natl. A. Sci. India B. , 116(38), 18848-18853, https://doi.org/10.1073/pnas.1904955116, 2019.

Zhou, S., Yu, B., and Zhang, Y.: Global concurrent climate extremes exacerbated by anthropogenic climate change, Sci. Adv., 9(10), eabo1638, https://doi.org/10.1126/sciadv.abo1638, 2023.

Zscheischler, J. and Fischer, E. M.: The record-breaking compound hot and dry 2018 growing season in Germany, Weather Clim. 520 Extreme, 29, 100270, https://doi.org/10.1016/j.wace.2020.100270, 2020.